



Ice core record of dust sources in the western United States over the last 300 years



S.M. Aarons^{a,*}, S.M. Aciego^a, P. Gabrielli^{b,c}, B. Delmonte^d, J.M. Koornneef^e, C. Uglietti^{b,f}, A. Wegner^{b,g}, M.A. Blakowski^a, C. Bouman^h

^a Glaciochemistry and Isotope Geochemistry Lab, University of Michigan, 1100 N. University Ave, Ann Arbor, MI 48109, USA

^b Byrd Polar and Climate Research Center, The Ohio State University, 108 Scott Hall, 1090 Carmack Road, Columbus, OH 43210, USA

^c School of Earth Sciences, The Ohio State University, 275 Mendenhall Laboratory, 125 South Oval Mall, Columbus, OH 43210, USA

^d Disat, University of Milano-Bicocca, Piazza della Scienza 1, Milan 20126, Italy

^e Vrije University Amsterdam, de Boelelaan 1085, 1081HV Amsterdam, The Netherlands

^f Laboratory of Environmental Chemistry, Paul Scherrer Institute, Villigen 5232, Switzerland

^g Stiftung Alfred-Wegener-Institut für Polar- und Meeresforschung, Am Alten Hafen 26, Bremerhaven 27568, Germany

^h Thermo Fisher Scientific, Hanna-Kunath-Str. 11, Bremen 28199, Germany

ARTICLE INFO

Article history:

Received 22 April 2016

Received in revised form 1 July 2016

Accepted 7 September 2016

Available online 12 September 2016

Keywords:

Dust

Ice core

Midlatitude glacier

Radiogenic isotopes

Trace elements

Paleoclimate

Dust cycle

ABSTRACT

Over the past ~5000 years, amplified dust generation and deposition in the American West has been linked to human activity. In recent decades, intensified rates of agriculture and livestock grazing have been correlated with greater dust production detected on seasonal to annual timescales. The combination of land use intensification and climate change (i.e. increased drought frequency) in North America highlights the importance of characterizing the sources of dust both before and after the influence of anthropogenic activity. We apply high-precision geochemical and isotopic (Sr and Nd isotopes) techniques to an ice core from the Upper Fremont Glacier (Wyoming, USA) to produce the first glacial dataset from the American West. Our Sr-Nd isotopic composition data indicates the evolving dust provenance to the Upper Fremont Glacier (UFG) from a long-range transport of mineral dust to a local source. This increasing input of dust from a local source is supported by a rise in average dust particle diameter combined with greater average dust concentration throughout the record. The greater presence of dust particles smaller than 2.5 μm in the most recent samples from UFG ice core record support existing satellite and sediment core data regarding the effects of anthropogenic activity upon dust sources and pathways in the American West. Although the Sr-Nd isotope database in North America needs to be expanded, our results provide a survey of windborne dust through the past 270 years.

© 2016 Elsevier B.V. All rights reserved.

1. Introduction

1.1. Background and motivation

Ice cores provide a continuous record of climate history and can capture a longer time period than modern, in-situ measurements and, when compared to lake sediments, ice cores are not contaminated with local sedimentary input derived from rivers (i.e. lake sediment studies). Midlatitude alpine glaciers are regional archives of climate providing insight into paleoclimate and paleoenvironmental conditions. The high accumulation rates preserve anthropogenic pollutant input at high temporal resolution (Schuster et al., 2002; Uglietti et al., 2015). Physical measurements of impurities (such as mineral dust) in the ice can provide insight into the regional and global climate conditions

through time (Delmonte et al., 2004a; Fischer et al., 2007; Wolff et al., 2006). In addition to particle size distribution, determining the sources and transport pathways of dust involves detailed studies of the mineralogy, elemental compositions, and radiogenic isotopic composition of dust entrained within ice and potential source areas (PSAs) (Delmonte et al., 2004a; Lupker et al., 2010; Thevenon et al., 2009). Here, we attempt to isolate the contributions of different sources of dust deposited on the midlatitude Upper Fremont Glacier (Fig. 1) in North America during the time period of 1720 CE to 1974 CE to document changes in the dust cycle throughout the increasing agricultural and industrial activity in the American West.

Dust deposition can impact terrestrial ecosystems by: (1) contributing to phosphorus deposition in the western US, leading to eutrophication of inland waters (Ballantyne et al., 2011), (2) altering the energy balance in mountain environments by accelerating melting rates of snow packs and alpine glaciers (Painter et al., 2007), and (3) shift regional hydrological cycles due to earlier melting (Painter et al., 2007).

* Corresponding author.

E-mail address: smaarons@umich.edu (S.M. Aarons).

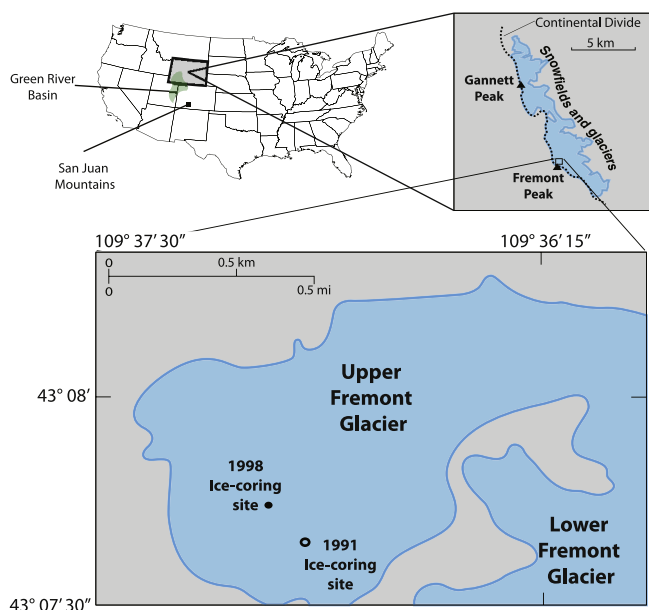


Fig. 1. Upper Fremont Glacier (UFG) location map with 1998 CE ice coring site (samples measured in this study) depicted by black circle and 1991 CE ice coring site depicted by open circle. Ice coring site is located within the Wind River Range, WY, east of the continental divide. Locations of potential source areas of dust from San Juan Mountains, Colorado (black square) and Green River Basin (green shaded area) are also noted. (For interpretation of the references to colour in this figure legend, the reader is referred to the web version of this article.)

Because the impacts of dust on ecosystems depend on the chemical compositions and thus source of the dust, understanding the dust sources and pathways in the American West is important to determine how both ecosystems and surface energy mass balance have evolved throughout time.

1.1.1. Global versus local inputs of dust

Dust fluxes are derived from both global (thousands of kilometers from the sink) and regional (tens to hundreds of kilometers) sources. Global sources (e.g. important deserts) are large places up to millions of square kilometers in area, generally arid, have an abundance of small particles and are subject to strong winds. The amount and impact of regional 'local' dust originating from anthropogenic activity (e.g. agriculture) is location-dependent and, in general, is believed to be less than the global contribution (Tegen et al., 2004), although this belief is not well quantified. Modern global dust emissions and corresponding source areas are observable via satellite (Ginoux et al., 2012; Prospero et al., 2002); major dust sources are the largest northern hemisphere deserts (North Africa, Middle East, and the high deserts of Asia). Dust is carried out of Asia eastward, with dust storm peaks in the spring (Prospero et al., 2002 and references therein).

Distinguishing between global (arid) and regional local dust is important due to ongoing land-use and climate change that will likely have a larger impact on local versus global dust transport and deposition. Increasing agriculture or aridity due to land-use change may create new sources of local dust, however the effects of climate change should dominate future dust emissions from well-characterized global dust sources (e.g. the Sahara, Gobi and Atacama deserts) (Tegen et al., 2004).

Shifts in average particle diameters can distinguish local from global dust. Far-traveled dust is typically $<10\ \mu\text{m}$ due to the effects of gravitational settling, and regionally sourced dust is typically $>10\ \mu\text{m}$ (Fig. 2) (Delmonte et al., 2004a; Mahowald et al., 2005). Glaciers at high altitudes and low latitudes can have deposited local/regional dust particles ranging from 3 to 12 μm (Uglietti et al., 2014). The lifetime of dust particles in the atmosphere is dependent on particle size, ranging from a few hours for particles larger than 10 μm , up to several weeks for

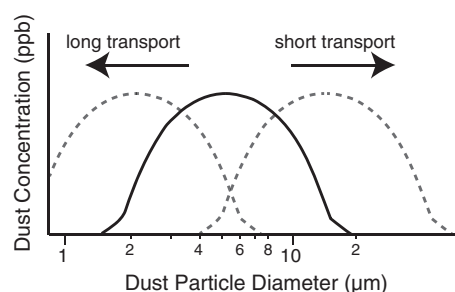


Fig. 2. Schematic of dust particle size distribution as an indicator of transport distance. Note that smaller (larger) dust particle diameters are indicative of long (short) transport distance.

submicrometer-sized particles (Mahowald et al., 2005). The threshold friction velocity, or the friction velocity a particle must pass before movement via saltation, increases with grain size due to gravity, but also increases for smaller particles due to particle cohesion, which results in an optimum particle size of $\sim 60\text{--}80\ \mu\text{m}$ at which the threshold friction velocity is at a minimum (Mahowald et al., 2005). Dust particles with sizes of $\sim 70\ \mu\text{m}$ are picked up most easily by winds, however, the dust transported thousands of kilometers has a modal diameter of $\sim 2\ \mu\text{m}$ (Mahowald et al., 2005; Schulz et al., 1998). Although long-range transported dust is typically small, larger dust particles ($>100\ \mu\text{m}$) have been recorded to travel long distances to remote oceanic regions (Betzer et al., 1988). Increases in dust concentration and average particle diameter may result from land use changes (Fig. 3), increased drought frequency, and higher than average wind speed, all of which culminate in greater dust emission and deposition (Ballantyne et al., 2011; Belnap and Gillette, 1997; Neff et al., 2008; Reheis and Urban, 2011).

To address the issue of increasing dust deposition related to anthropogenic activity in the western United States, several studies utilize dust particles in lake sediment cores and mountain snowpack (Brahney et al., 2014; Brahney et al., 2013; Doebbert et al., 2014; Neff et al., 2008). Dust particles in lake sediment cores are operationally defined as up to 65 μm in diameter, while dust in ice cores is generally smaller (Brahney et al., 2014, 2013; Doebbert et al., 2014; Neff et al., 2008). The primary method of distinguishing between long range transported dust to a locally derived source is particle size distribution. Neff et al. (2008) defined a 37–63 μm grain size fraction as eolian derived and the $>250\ \mu\text{m}$ as locally eroded bedrock. Additionally, Neff et al. (2008), measured particle-size distribution for modern dust for 5 different dust deposition events, with the results showing that 40% of dust mass collected occurs in the 10–37 μm class, 26% in the 37–63 μm class, and 17% in the 63–180 μm class. The authors speculated that the relatively large proportion of particles $>37\ \mu\text{m}$ is evidence for particles that have been transported hundreds rather than thousands of kilometers (Middleton et al., 2001; Neff et al., 2008). Similarly, Ballantyne et al. (2011) studied lake sediments in two size classes: 37–60 μm and $>250\ \mu\text{m}$. The smaller size class most closely resembled the particle size distribution of eolian dust, whereas the larger size class was most likely locally derived sediment (Ballantyne et al., 2011). In order to discern changes in finer dust particles from regional sources ($>10\ \mu\text{m}$) versus globally sourced dust ($<10\ \mu\text{m}$), we utilize the Upper Fremont Glacier ice core as a paleoclimate record that is relatively pristine and does not contain sediment input from bedrock weathering.

Regionally, the largest modern, documented dust sources in North America lie between the Sierra Nevada Mountains to the west, and the Rocky Mountains to the east (Prospero et al., 2002). There is seasonal variability in the export of dust from these regions, with dust transport generally highest from April through September. Human activity can result in greater dust availability over time, and studies show that the number and magnitude of dust sources in the American West region has increased as a result of anthropogenic activities (Grayson, 1993;

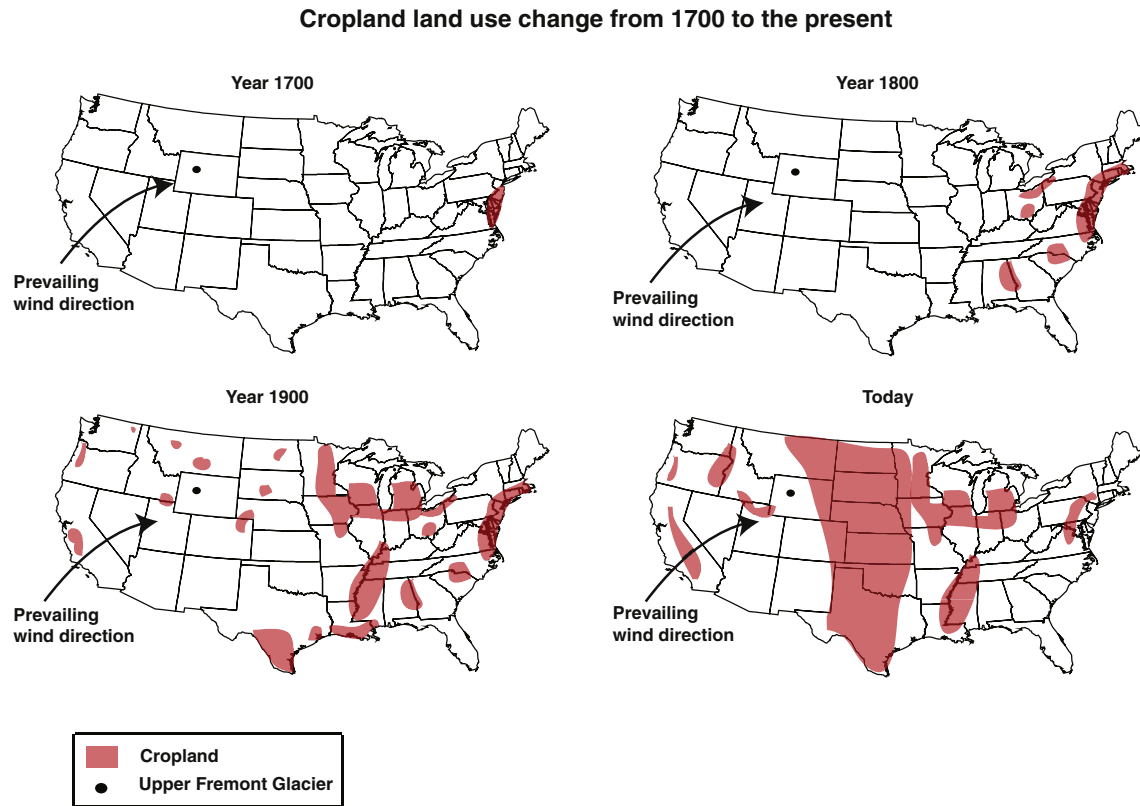


Fig. 3. Historical land use maps for the United States during the time periods of 1700, 1800, 1900 and today (adapted from Goldewijk, 2001). Also shown are the prevailing wind direction and location of the Upper Fremont Glacier.

Reheis, 1997). While the Great Plains was a major dust source during the 'Dust Bowl,' modern observations do not show this region as a significant dust emitter compared to natural or other human-caused sources of dust in North America (Prospero et al., 2002).

1.1.2. Anthropogenic influence on dust cycle

Anthropogenic dust sources are closely linked to the hydrological cycle, as satellite observations indicate emissions are correlated to land use and proximity to short-lived bodies of water (Ginoux et al., 2012). In areas with low precipitation rates, agriculture and livestock grazing disturb soils and vegetation, leaving soils more susceptible to wind erosion during drought periods (Prospero and Lamb, 2003). Increased human activity (i.e. agriculture and livestock grazing) in the American southwest and the Colorado Plateau during the past several decades has been correlated with greater dust production and deposition, which has been detected on mountain snow cover on seasonal to annual timescales (Neff et al., 2008; Painter et al., 2007; Reynolds et al., 2001). We would expect to observe higher concentrations of larger dust particles ($>10\ \mu\text{m}$ in diameter) in the ice core record as agriculture and livestock grazing increases due to amplified dust generation and availability for transport. On longer timescales, the magnified impact of evolving agricultural practices (industrialization, soil conservation and increased cultivation area) on the dust cycle across North America has not yet been explored using ice core records. Land use dramatically changed from the time of initial European exploration, immigration, and agricultural cultivation as waves of immigrants settled the Great Plains and the American southwest (California, Nevada and Arizona). From the 1700s to the present, the expanse of cultivated cropland across the US has increased by several orders of magnitude (Fig. 3). Soil conservation efforts throughout the US following the Dust Bowl in the 1930s should result in a diminishing presence of large diameter dust particles in the ice core record, as coarser (sandy) particles are

more susceptible to wind erosion than finer (silt and clay) particles (Lyles, 1985).

During the period of pre-Industrial and pre-expansion into the American West (1720–1820 CE), natural changes in dust concentration and size distribution should coincide with regional droughts. Dry, arid conditions lead to higher dust availability, which combined with a mechanism for transport (wind), will lead to dustier conditions. Larger dust particles ($>10\ \mu\text{m}$) are likely regionally sourced dust, whereas smaller dust particles ($<10\ \mu\text{m}$) are far traveled dust transported in the upper troposphere (Fig. 2). During the Second Industrial Revolution (1860–1910 CE) and the westward expansion (~1869 CE), intensive grazing in certain parts of the West increased, and we would therefore expect to see increases in dust concentration and average dust particle diameter as the dust is regionally sourced. During the Dust Bowl (~1930 CE), severe drought combined with little to no crop rotation would result in an increase of transportable dust. Dust deposited during the dust bowl has been observed in the Greenland ice core record (Donarummo et al., 2003), and in the UFG record should be in the diameter range of $1.2\text{--}4\ \mu\text{m}$, consistent with a soil-derived source (Patterson and Gillette, 1977). The droughts that affected North America during 1950 CE and the late 1980s CE combined with higher wind speeds during the spring would likely cause an increase in coarse-grained particles transported to sinks in close proximity (e.g. lakes and mountain glaciers). From 1970 CE onward, increased activity such as agriculture and livestock grazing in the American southwest and Colorado Plateau would result in greater dust production and a shift in dust provenance to these regions depending on the wind direction.

Recent work (Brahney et al., 2014, 2013; Doebbert et al., 2014; Neff et al., 2008; Painter et al., 2007) has indicated that agriculture development and water diversion has resulted in larger, local dust emissions from the Colorado Plateau and Green River Basin. Because of the growing interest in using ice cores from alpine glaciers to reconstruct records

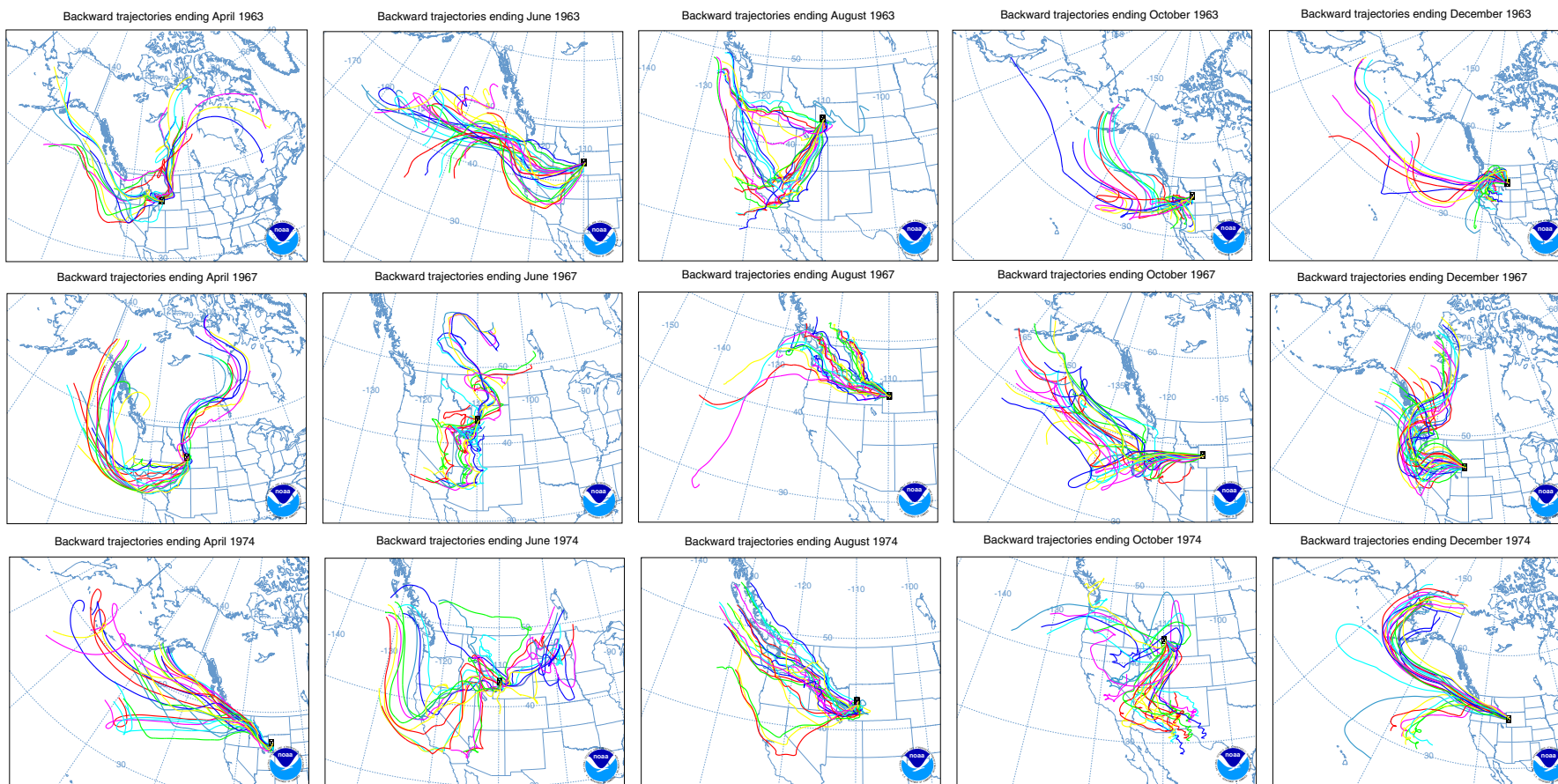


Fig. 4. NOAA HYSPLIT air parcel backward trajectory model for UFG coring site. Back trajectory model at 4000 m elevation and meteorological conditions for April, June, August, and December 1963, 1967, and 1974 CE respectively (Draxler and Hess, 1998); these model conditions reveal backward trajectories from a wider sector of western North America, including Colorado, New Mexico, and Arizona, and western Arctic Alaska and Canada. This figure was generated using the NOAA Hybrid Single-Particle Lagrangian Integrated Trajectory (HYSPLIT) model, which computes air parcel trajectories to demonstrate dispersion and deposition pathways (Draxler and Hess, 1998).

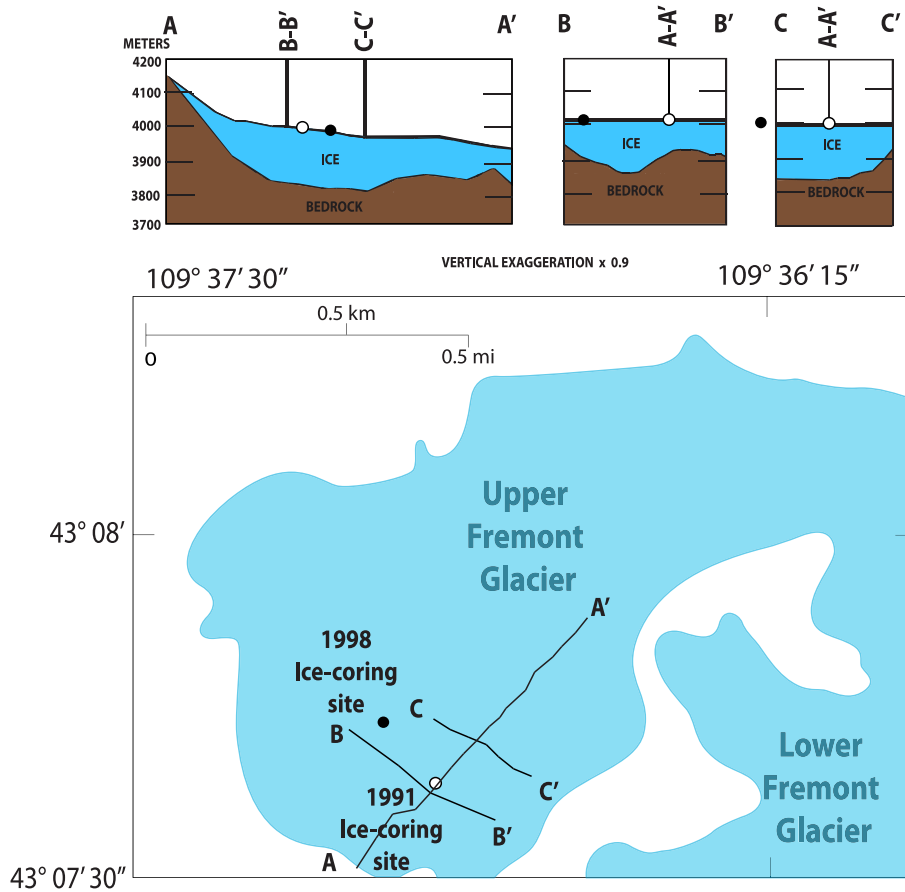


Fig. 5. Ice thickness cross sections. Ice thickness along three transects on the Upper Fremont Glacier, Wyoming. Also shown are approximate ice core locations in 1991 (open black circle) and 1998 (closed black circle) respectively. (Figure adapted from Naftz et al., 1996).

of dust sources and deposition, we must also consider changes in rock exposure due to the advance or retreat of glaciers over time. For example, at the UFG site, fresh moraine or more likely outwash material could be an increasing local source over time due to the retreat of the seven glaciers in the Wind River Range (WRR) since the Little Ice Age (LIA), and should be $> 10 \mu\text{m}$. These moraines are essentially devoid of vegetation; thus, if up-glacier winds are strong enough, they could pick up glacier flour particles from these moraines. Outwash plains can be a source of windblown dust because the constant grinding of glacial processes produces glacial flour, which is fine-grained crushed bedrock. Braided streams are constantly moving across the outwash plain, leaving behind unconsolidated sediment exposed to wind. Dust from these glacial processes is uplifted into the atmosphere by wind gusts and transported tens to thousands of kilometers depending on the dominant wind direction and strength. Previous work has linked dust flux peaks in Antarctica with periods of high sediment deposition in outwash plains in Patagonia (Sugden et al., 2009), and it is therefore important to consider moraine or outwash material as significant contributors to dust in ice cores.

1.1.3. Satellite observations of dust transport

In tracking modern dust emissions and modeling transport for the purposes of determining air quality, dust source activations (DSAs) are well defined (Schepanski et al., 2007, 2009). However, in paleoclimate literature DSAs are not known but hypothesized, and are therefore referred to as PSAs (Basile et al., 1997; Biscaye et al., 1997; Delmonte et al., 2010, 2004a; Mahowald et al., 1999). In order to narrow the possibilities of PSAs globally and regionally, we used the web-based version of the NOAA HYSPLIT model (HYbrid Single-Particle Lagrangian Integrated Trajectory Model, 1997, <http://www.arl.noaa.gov/ready/>

[hysplit4.html](http://www.arl.noaa.gov/ready/hysplit4.html)) to illustrate the range in isentropic backward air trajectories terminating at the ice core site on the UFG (Fig. 4). The HYSPLIT

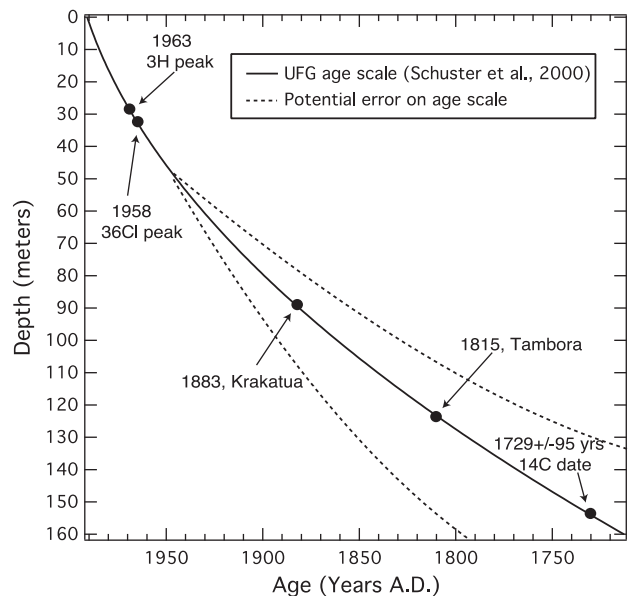


Fig. 6. Age-depth profile. 1991 UFG ice core age and depth relationship based upon chemical and volcanic tie points. Solid black line represents the polynomial fit for the age-depth profile, dashed black lines represent potential error of age-depth relationship. (Figure adapted from Schuster et al., 2000).

model computes air parcel trajectories to demonstrate dispersion and deposition pathways (Draxler and Hess, 1998) using publicly available model-derived meteorological data formatted for HYSPLIT from NOAA ARL (www.ready.noaa.gov/archives.php) and NOAA NCEP (<ftp://ftpprd.ncep.noaa.gov/pub/data/nccf/com/hysplit/prod/>). Seven-day back trajectories were performed using known meteorological conditions for the second week in April, June, August, October, and December 1963, 1967 and 1974 CE, respectively. We chose these years as they are the approximate ages of several samples from the UFG ice core record measured here, these months to span a large portion of the year and to determine any seasonal trends, and the week randomly. Even with these fifteen model runs (Fig. 4), it is apparent that air masses from all modern dust emission sources in North America can be transported to the UFG site. Because back trajectory models require recorded meteorological conditions to run, it is not possible to determine trajectories during the entire time period of ice covered by our ice core (except for 1963, 1967, and 1974 CE), and so we use these for illustrative purposes to show monthly, seasonal and annual variability. It is important to note that backward trajectories provide insight into dust pathways, however the mixing of multiple dust sources in the atmosphere is complex and difficult to model.

1.2. Upper Fremont Glacier site description

The glaciers of the WRR experience generally low solar radiation and predominantly westerly winds due to the easterly orientation (Fryxell, 1935). The average annual precipitation from 1971 to 2000 at the WRR is 1143 mm/year (of water equivalent) (Curtis and Grimes, 2004), with the majority of precipitation occurring as snow during the winter. Wyoming has experienced both higher annual temperatures and precipitation on a decadal basis since 1966 (Curtis and Grimes, 2004), and reconstructed air temperatures based on water stable isotope data from the UFG ice core indicate an increase in average air temperature of $\sim 5^\circ\text{C}$ from the end of the LIA to the early 1990s (Naftz et al., 2002). Two $\sim 160\text{ m}$ long ice cores were drilled in 1991 and 1998 at the UFG, providing the first successful reconstruction of paleoclimate from a south-central North American ice core (Naftz et al., 1996). These records include stable oxygen isotopes in precipitation, nitrate and tritium concentrations, and carbon-14 concentration from grasshopper leg parts entrained in the ice, sulfate, chloride, and electrical conductivity measurements, and Hg concentrations (Naftz et al., 1996; Schuster et al., 2002, 2000). Thus far, these records show the impact of warming climate and industrialization as the precipitation trends toward heavier

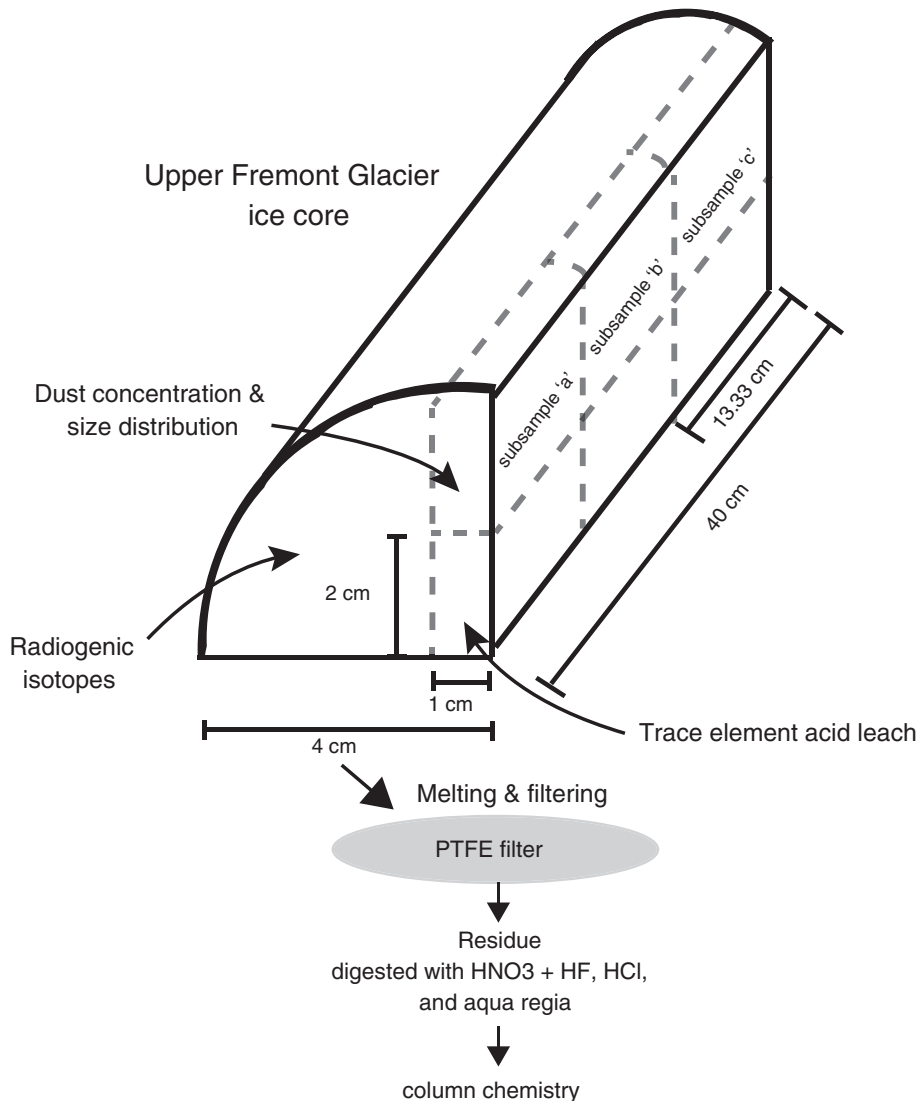


Fig. 7. Schematic of ice core sample preparation for radiogenic isotope, dust concentration and size distribution, and rare earth and trace element analysis of UFG ice core.

oxygen isotopic values and higher atmospheric concentrations of Hg are observed over the time encompassed by the ice core. For this study, we used samples from the UFG core drilled in 1998, as the 1991 UFG core was almost entirely consumed for previous work. The 1998 UFG core drilling location is within 200 m of the 1991 core.

The high altitude of the UFG minimizes the occurrence of meltwater percolation and re-freezing (Naftz et al., 2002), however percolation and washout is possible, which is why the filtrate portion of the UFG ice core was not measured. The insoluble particles and trace element (TE) records should not be affected by meltwater percolation, as recent work by Wong et al. (2013) indicates that the seasonal chemical signal is preserved during meltwater intrusion. Furthermore, Wong et al. (2013) showed that dust TEs retain their annual stratigraphy and are capable of serving as a dating parameter in ice cores affected by up to 10% annual melt, and assuming that the UFG did not exceed this melt index, melt events should not significantly affect the age scale and interpretation of the UFG ice core.

2. Materials and methods

We analyzed 13 samples from the UFG ice core (FRE 98-4 ice core, 43°07'37" N, 109°36'54" W, 4000 m a.s.l.), located in the WRR, Wyoming, USA (Fig. 1). Ice core samples from the UFG were delivered from the National Ice Core Laboratory (NICL). The ice core samples measured during this study spanned a depth of ~158–20 m below the surface corresponding to the time interval ~1715–1974 CE. Each ice core section was approximately 40 cm long and span ~1 year. Each ice core section was cut longitudinally into 3 subsamples: the outer portion for radiogenic isotopic composition measurement, another for dust concentration and size distribution measurements, and the last for TE concentration determination. Hereafter, the procedure for processing the radiogenic samples varied from the processing for the dust concentration and size distribution and TE samples using previously published methods (Koorneef et al., 2014).

2.1. Age scale and uncertainty between 1991 and 1998 UFG ice core

Two ice cores from the Upper Fremont Glacier were retrieved from two different sampling locations in 1991 and 1998 CE, respectively (Fig. 5). The two ice cores encompass the same time period; the age/

depth relationship is slightly different, but not systematically over the entire records. Uncertainty in the age scale is as high as 95 years (based on a carbon-14 date) at the base (~1715 CE), and 10 years near the surface. We apply the age scale of the 1991 core to the 1998 core for this study, as the 1998 core possesses oxygen isotope data only for the depths of 16–60 m (Schuster et al., 2004). It should be noted, that the oxygen isotope data from the 1991 and 1998 core agree with each other.

Previous work (Schuster et al., 2002) utilized both the 1991 and 1998 ice cores to produce a single atmospheric mercury deposition record in North America from ~1720 to 1993 CE. The continuity of the Hg record between the two separate UFG ice cores suggests that the chronology displacement of the records is sub decadal. Annual dust layers in the UFG are not always present, making visual layer counting as a method of age dating impossible. The chronology of the 1991 UFG was determined using chemical and isotopic age dating techniques. The 1963 tritium (Naftz et al., 1996) and 1958 chlorine-36 peaks (Cecil and Vogt, 1997; Naftz et al., 2002) were located at depths of 28 and 32 m, respectively. A carbon-14 value obtained from a grasshopper leg entrained in ice at 152 m yielded an age of 221 ± 95 years BP (Naftz et al., 1996). These dates, along with the estimated snow accumulation and ablation values (Naftz, 1993), were used to establish a low-resolution age scale for the UFG cores.

Additional volcanic time markers for the ice cores were established at depths of 88 and 123 m using electrical conductivity measurements, which improved the ice-core chronology to prediction limits of ± 10 years (90% confidence level) (Schuster et al., 2000). The lack of concrete chemical age-markers below the depth of 32 m suggests that the age scale for the 1991 core possesses a potential error, which may be significant with increasing depth (Fig. 6). Unfortunately we are unable to precisely calculate the potential error on the age scale and we use the dashed lines on Fig. 7 to illustrate this uncertainty. The potential error has implications for samples at higher depths, and highlights the necessity of accurately determining the 1998 UFG ice core age scale. The tritium peak in the 1998 ice core is ~1.5 m deeper than the tritium peak in the 1991 ice core (Naftz et al., 2002), most likely due to additional snow deposited on the UFG between the 1991 and 1998 ice core retrievals and small-scale variations in snow accumulation and retention between the two sites. Additionally, changes in ice flow and redistribution could be potential sources of the offset in depth of the tritium peak

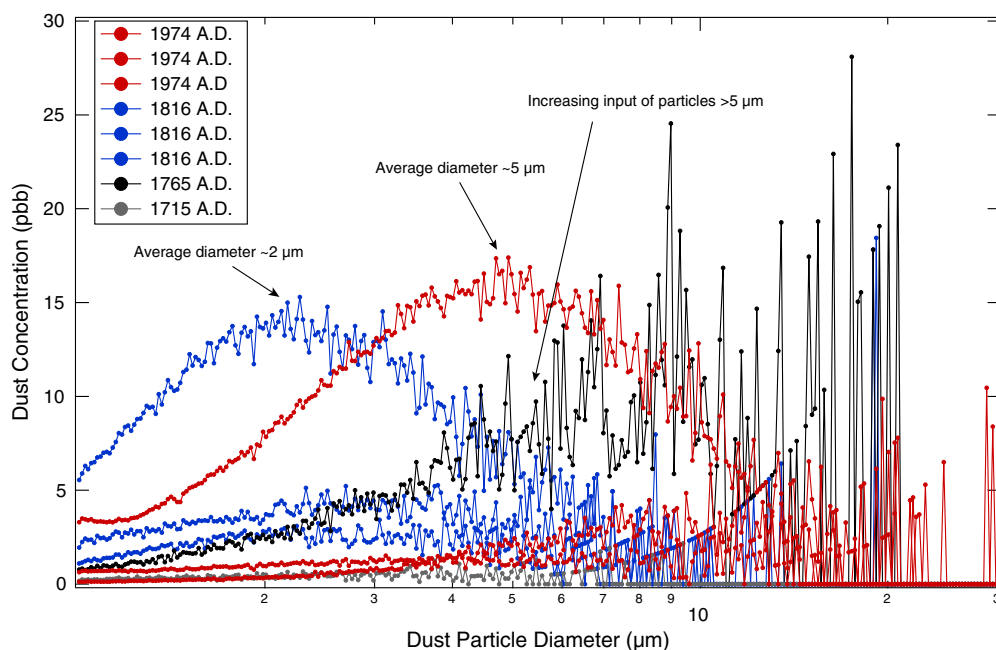


Fig. 8. Dust particle size distribution. Dust concentration (ppb) with respect to dust particle diameter (μm) for subsamples from time periods of 1715, 1765, 1815, and 1974 CE.

between the two ice cores. Although ice folding is a possibility, previous studies have indicated that there is no evidence of this (Schuster et al., 2002), and the upper 60 m of the 1998 ice core are well dated (Schuster et al., 2004). Radio-echo sounding used to determine ice thickness at the UFG did not suggest the occurrence of ice folding (Naftz, 1993). Although seasonal isotopic signatures should not be preserved, long-term trends in climate are visible, which is sufficient for describing changes in dust provenance over the time record considered.

The 1991 UFG ice core is ~160 m long with ~270 years of paleoclimate record, suggesting an average accumulation rate of >0.5 m/year ice equivalent. Based upon the accumulation rate and the unlikely possibility of significant ice thinning in the relatively shallow alpine glacier, we estimate that the timescale difference between the 1991 and 1998 ice cores are likely sub-decadal. Each sample measured in this study was ~0.4 m in length, representing at least one year and even longer at greater depths depending on the rates of ice thinning. However, despite the possibility of a sub-decadal difference in age, the overall age scale should be sufficient for the purposes of investigating changes over 250 years.

To examine potential differences in ice stratigraphy between the two ice core sites, we also incorporate the ice thickness data of three transects of the UFG determined using radio-echo sounding (Fig. 5) (Naftz et al., 1996), which was confirmed by drilling to bedrock in 1991 (Naftz, 1993). The two ice core sites from 1991 and 1998 are in close proximity to the transect B–B', indicating that the two ice cores retrieved are of similar thickness (~160 m), and are situated close to the accumulation area without any major bedrock anomalies that would result in a major disturbance to the age-scale relationship between the two ice cores (see transect A–A') (Fig. 5). Chronological refinement on the age-depth relationship of the 1991 UFG ice core utilized volcanic events, and isotope and chemical data (Schuster et al., 2000). A best-fit polynomial line was fitted to this data and plotted (Fig. 6), and the age equation (Schuster et al., 2000) is:

$$\text{Age in years} : 0.00738 (D)^2 + 0.5558 (D)$$

where 'D' is depth in meters. We applied this age-depth relationship equation to determine the approximate age of samples from the 1998

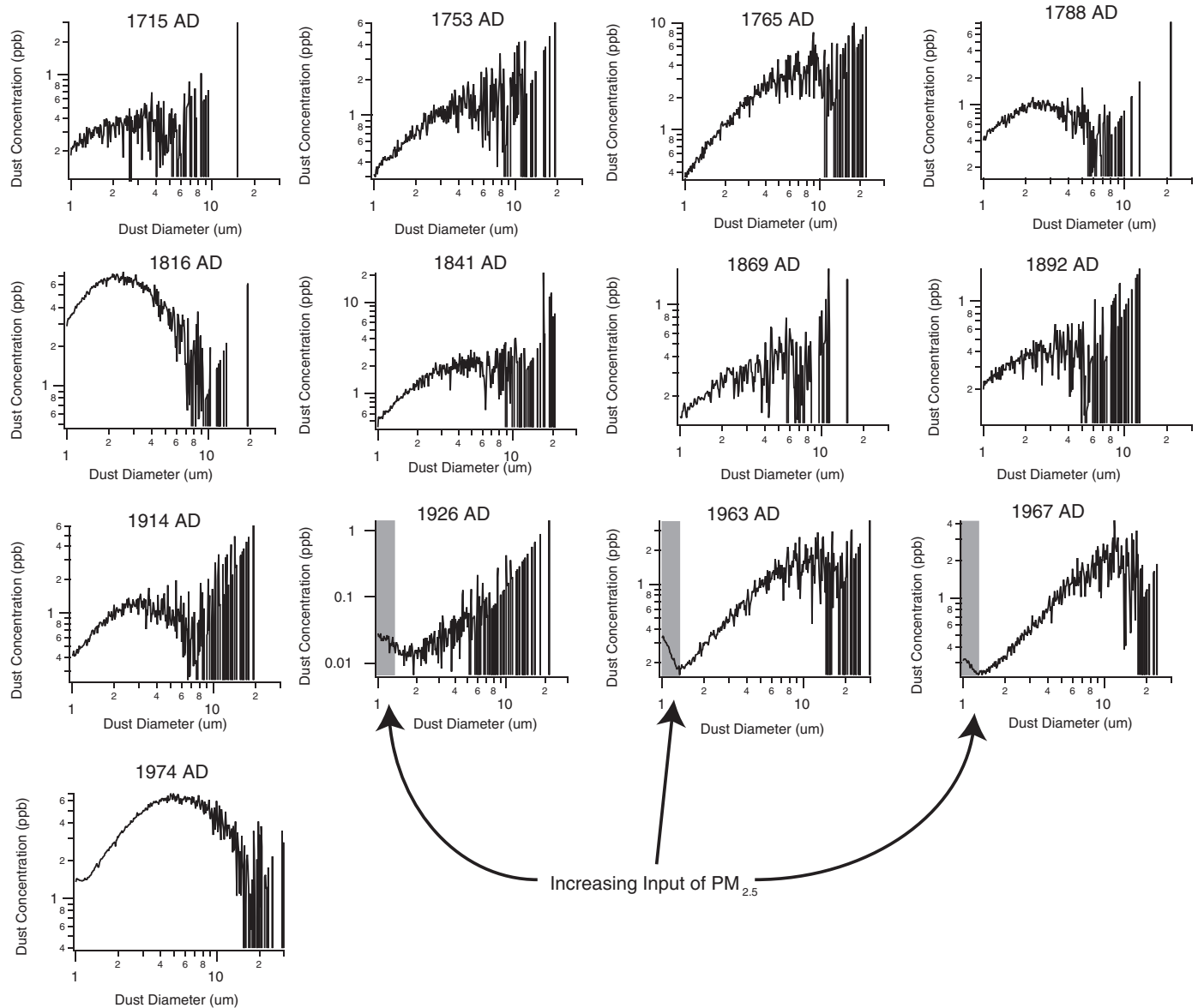


Fig. 9. Dust particle size distribution. Dust concentration (ppb) with respect to dust particle diameter (um) for all samples from Upper Fremont Glacier. Note the shaded area in samples 1926, 1963, and 1967 CE highlights the increasing input of particles <2.5 um.

UFG ice core, and based upon the proximity of the two drilling locations, the maximum offset between the two ice core records should be <10 m; which will result in an age offset that increases with increasing depth. Thus, if we assume that the maximum depth offset between the two ice cores is 10 m, and that the 1991 age scale equation is correct, then the age offset would be <30 years between the two ice cores, which is insignificant in terms of the trends discussed here.

2.2. Initial processing and decontamination of the UFG ice core

From the three 40 cm long subsamples, the outer portion was reserved for radiogenic isotopic composition measurement (weighing approximately 314 g), along with one section for dust concentration and size distribution measurements (weighing approximately 73 g), and one for TE concentration measurement (weighing approximately 73 g). The latter two samples were split into three subsamples: a, b, and c (each weighing approximately 24 g), with subsample “a” being the portion of the core closest to the surface of the glacier (see Fig. 7 for a schematic of the ice core cutting diagram). Tools for decontaminating and processing the ice core were made of PFA Teflon and acid washed prior to use; we used PFA Teflon chisels impregnated with quartz to scrape the outermost layer of the ice. All initial processing and chemistry were performed in a class 10,000 clean room, under class 100 laminar flow hoods.

2.3. Processing of the radiogenic isotope portion of the UFG ice core

Each ice core sample for the radiogenic portion was decontaminated using a three-step procedure. First, while the ice core sections were still cold ($-25\text{ }^{\circ}\text{C}$), the outer most 2 mm were scraped with the PFA chisels and then rinsed with distilled ethanol. After allowing the ice cores to

warm up for ~ 10 min, the cores were again scraped another 1–2 mm with a new, clean PFA chisel, and rinsed with MilliQ water. The core sections were then melted while buffered to a neutral pH with ultra-pure ammonia, and the resulting liquid was immediately filtered through 2 acid pre-cleaned $0.2\text{ }\mu\text{m}$ and $30\text{ }\mu\text{m}$ Teflon filters under a class 100 laminar flow hood. The dust fraction was dissolved and digested off the filters for elemental separations using column chemistry procedures described in Lupker et al. (2010).

Sr and Nd fractions of particularly dusty (~ 0.5 dust mg yield after filtering) UFG ice samples were analyzed using a Thermo Scientific Triton PLUS Thermal Ionization Mass Spectrometer (TIMS) equipped with 10^{11} Ohm resistors at the University of Michigan, while the small Nd fractions were analyzed using a Thermo Scientific Triton PLUS TIMS equipped with 10^{13} Ohm resistors at VU Amsterdam using procedures described by Koornneef et al. (2014). All Sr isotopic compositions were normalized to $^{88}\text{Sr}/^{86}\text{Sr} = 8.375209$ to correct for mass bias, and the Sr isotopic standard SRM987 (10 ng) was also measured at $^{87}\text{Sr}/^{86}\text{Sr} = 0.710269 \pm 5$ (2σ SD, $n = 5$) on the University of Michigan Thermo Scientific Triton PLUS (Table 2). The USGS reference material BCR-2 (10 ng) measured at the same time as the samples averaged 0.705035 ± 7 (2σ SD, $n = 1$) (Table 2). Neodymium isotopic compositions were normalized to $^{146}\text{Nd}/^{144}\text{Nd} = 0.7219$ using the exponential law and mass 149 was monitored for Sm interference. To ensure accuracy, Nd isotopic standard JNdi-1 (10 ng) was measured at $^{143}\text{Nd}/^{144}\text{Nd} = 0.512102 \pm 22$ (2σ SD, $n = 4$) (Table 2).

We measured two different size fractions (fine filter: $0.2\text{--}30\text{ }\mu\text{m}$, and coarse filter: $30\text{--}60\text{ }\mu\text{m}$) of particulates collected from the filtered and buffered meltwater of 13 discrete samples from the 1998 UFG ice core for Sr and Nd isotopic composition. Next, we performed bulk analysis of dust concentration and size distribution and TE concentrations on three longitudinal subsamples for each primary sample to assess short

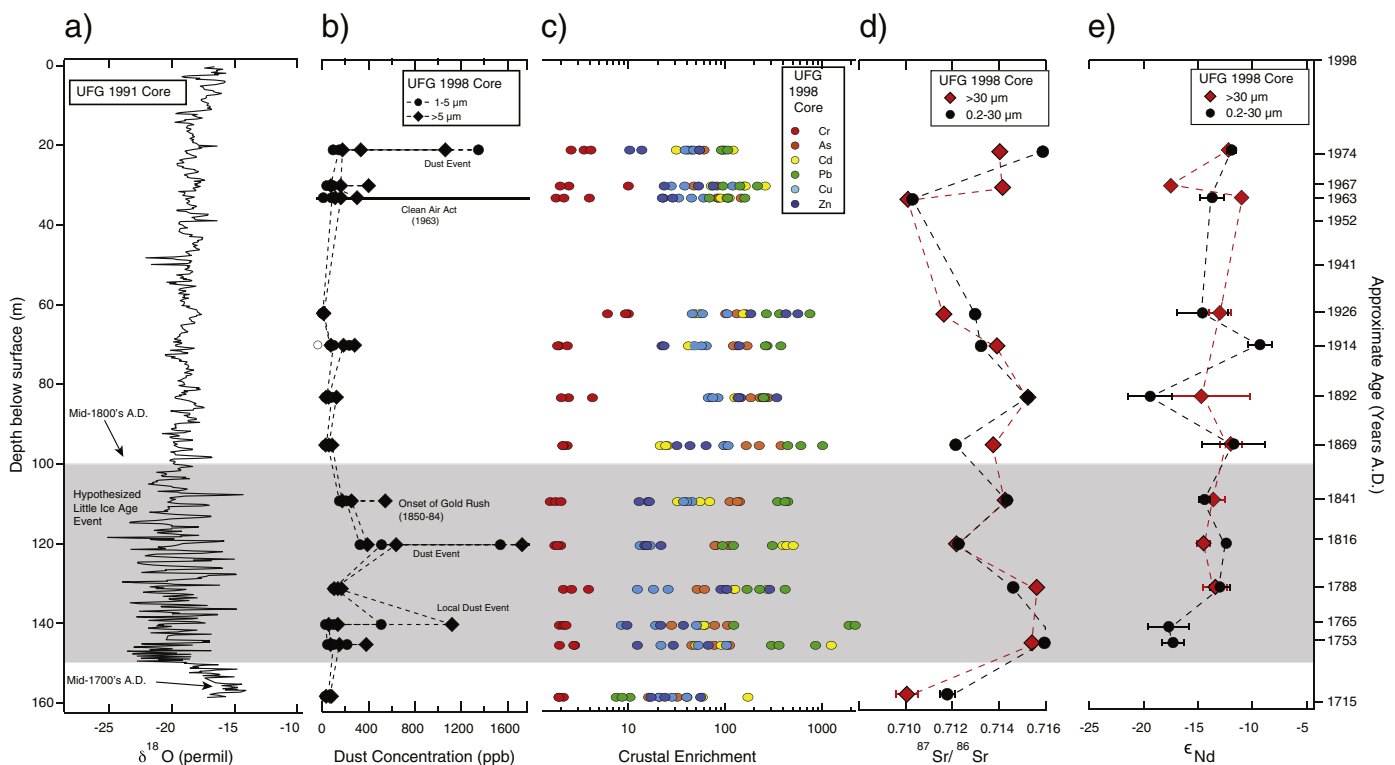


Fig. 10. Isotope, dust concentration and trace element records. a) $\delta^{18}\text{O}$ from 1991 UFG ice core meltwater (Naftz et al., 1996). b) Dust concentration from FRE 98-4 separated into 1–5 (μm) (black circles) and $>5\text{ }\mu\text{m}$ (black diamonds). c) Crustal enrichment of FRE 98-4 meltwater for the trace metals Cr, As, Cd, Pb, Cu and Zn, common industrial pollutants (circles distinguished by colour, see legend; see Table S1 for concentrations of all trace elements analyzed). d) $^{87}\text{Sr}/^{86}\text{Sr}$ and e) ϵ_{Nd} for $0.2\text{--}30\text{ }\mu\text{m}$ (black circles) and $>30\text{ }\mu\text{m}$ (red diamonds) insoluble dust. (For interpretation of the references to colour in this figure legend, the reader is referred to the web version of this article.)

term (<1 year) variability. Melted ice core samples were analyzed for dust concentration and size distribution by Coulter® Counter.

2.4. Processing of the trace element portion of the UFG ice core

Samples reserved for TE concentration analysis were triple-rinsed with MilliQ water using acid-washed LDPE pliers, and melted in pre-cleaned LDPE Nalgene bottles following procedures established by Boutron et al. (1990). The melted samples were immediately acidified in 1% HNO₃ (ultra-pure) and left to sit for approximately 1 month prior to analysis to dissolve dust particles (Uglietti et al., 2014). Trace element concentrations were determined at The Ohio State University on a Thermo Element2 Inductively Coupled Plasma Sector Field Mass Spectrometer (ICP SFMS) coupled with a micro-flow nebulizer and a desolvation system (Apex Q). This system allows for TE detection down to the sub-pg g⁻¹ levels (Uglietti et al., 2014). Low resolution (LR) mode was used for the detection of ⁸⁵Rb, ⁹⁵Mo, ¹⁰⁹Ag, ¹¹¹Cd, ¹²⁰Sn, ¹²¹Sb, ²⁰⁵Tl, ²⁰⁸Pb, ²⁰⁹Bi, and ²³⁸U, medium resolution (MR) mode for ²⁷Al, ⁴⁸Ti, ⁵¹V, ⁵²Cr, ⁵⁵Mn, ⁵⁶Fe, ⁵⁹Co, ⁶³Cu, and ⁶⁴Zn, and high resolution mode for ⁷⁵As.

2.5. Processing of the dust concentration and size distribution portion of the UFG ice core

The dust concentration and size distribution samples were triple-rinsed with MilliQ water using acid pre-cleaned LDPE pliers and stored in triple rinsed PTFE centrifuge tubes frozen until just prior to analysis following the procedures described in Delmonte et al. (2004a). For each dust concentration and size distribution subsample, ~20 ml was available for Coulter Counter Multisizer 3® microparticle concentration and size distribution measurements in the range of 1.006–29.83 μm. Five consecutive measurements were performed on each sample to ensure the accuracy of the results. The reproducibility is very good for concentrated samples (typically <2% for 50,000 particles/g), whereas some scattering occurs with low concentration samples (~20% for 1000/g) (Delmonte et al., 2002). The blank levels were negligible on the order of 1–2 ppb.

3. Results and discussion

3.1. Dust particle concentration and size distribution

Dust particle concentrations and size distributions are summarized in Figs. 8, 9, and 10b, respectively. The three sub-samples span a length of ~13.3 cm, and sub-samples from 1816 and 1974 CE have variable dust concentration and size distributions (Fig. 8). The difference in dust concentration and size is most likely due to a seasonal effect as the average annual accumulation rate is >0.5 m ice equivalent (note that dust concentration and size distribution of three sub-samples are averaged in Fig. 9). The average dust concentration changes from ~15 to 17 ppb from 1816 to 1974 CE, supporting the idea of amplified dust availability and/or dust events during that time period (Fig. 8) (Ballantyne et al., 2011; Belnap and Gillette, 1997; Delmonte et al., 2004a; Neff et al., 2008; Reheis and Urban, 2011). The uncertainty in dust concentration measurements ranges from 20% for low concentration (i.e. <10 ppb) to 2% for high concentration (i.e. >100 ppb) (Delmonte et al., 2002). We observe the highest dust concentration (>1600 ppb) at an ice depth of ~120 m below surface (~1816 CE), while the dust concentration is >1200 ppb at a depth of ~20 m below surface (~1974 CE) (Figs. 9, 10b). The average dust particle diameter of 5 μm (Fig. 8) associated with the high dust concentration observed in ~1974 CE suggests that this dust could not be transported over very large distances but originates from a local dust event near the UFG. The noticeably higher spikes in dust concentration are in the >5 μm dust fraction (Fig. 10b), suggesting dust deposition from local dust events. The larger observed dust sizes (>10 μm and <37 μm) recorded and analyzed in lacustrine

systems (Ballantyne et al., 2011; Neff et al., 2008), together with this data highlights the relevance of evaluating dust size fractions up to 60 μm when investigating continental dust records. When comparing older (1816 CE) to younger (1974 CE) samples, the average diameter of dust particles changes from ~2 μm to 5 μm (Fig. 8), suggesting either a shift to a closer dust source or increasing wind strength. The full record of dust particle size distribution with respect to dust concentration is shown in Fig. 9, illustrating the variable physical dust composition over the time period of interest.

3.2. Increasing input of PM_{2.5}

There is no clear trend in dust particle diameter size over time. Several of the younger samples (1926, 1963, and 1967 CE) have size distributions with the possibility of increasing input of particulate matter (PM) smaller than 2.5 μm (PM_{2.5}) (Fig. 9). However, the majority of dust mass deposited during these time periods is in the larger dust diameter size (>4 μm), suggesting increased levels of local dust input (i.e. larger particle diameter size), though the small spikes in PM_{2.5} are clearly visible in the dust particle size distributions (Fig. 9). Primary production of fine and ultrafine PM are both natural and anthropogenic in origin, and sources of particulate pollution may be from factories, power plants, refuse incinerators, motor vehicles, construction activity, fires and windblown mineral dust (Kampa and Castanas, 2008). Fine particles <2.5 μm in diameter may be damaging to human health through inhalation and accumulation in the respiratory system (Kampa and Castanas, 2008). The increasing abundance of particles

Table 1

Trace element enrichment factors. Enrichment factors (EF) of trace metals from UFG ice sample meltwater.

Top depth (m)	~Age (yrs A.D.)	Sample ID	Cr EF	As EF	Cd EF	Pb EF	Cu EF	Zn EF
20.29	1974	21a	3.5	60.4	53.9	98.8	41.2	13.7
20.29	1974	21b	2.6	44.8	31.3	91.3	38.6	10.3
20.29	1974	21c	4.1	93.3	120.5	106.0	47.2	54.3
29.81	1967	30a	2.4	82.3	160.8	141.7	38.1	23.4
29.81	1967	30b	2.0	47.4	71.9	94.5	27.6	53.0
29.81	1967	30c	9.9	154.9	258.9	215.4	119.5	75.2
33.36	1963	33a	3.9	146.5	109.6	159.3	59.7	22.8
33.36	1963	33b	1.8	82.8	90.1	68.3	32.8	22.4
33.36	1963	33c	2.1	85.3	104.6	106.1	44.9	28.5
62.36	1926	62a	9.9	101.2	48.5	266.0	45.6	183.9
62.36	1926	62b	6.1	164.3	54.5	749.1	58.1	561.5
62.36	1926	62c	9.3	131.7	153.7	364.1	105.1	425.5
70.25	1914	70a	1.9	168.2	48.7	376.0	63.6	22.1
70.25	1914	70b	1.9	132.4	47.1	270.7	56.7	23.3
70.25	1914	70c	2.3	121.2	41.7	259.6	48.4	139.3
84.42	1892	83a	4.2	183.9	125.9	244.9	66.7	341.1
84.42	1892	83b	2.4	229.2	135.8	256.5	84.1	144.3
84.42	1892	83c	2.0	276.9	70.4	247.9	74.2	137.9
95.87	1869	95a	2.3	378.3	25.3	1014.7	98.6	63.3
95.87	1869	95b	2.1	224.0	21.3	604.2	96.8	43.2
95.87	1869	95c	2.1	164.4	24.2	441.6	107.1	31.6
109.16	1841	109a	1.6	111.8	68.9	443.2	45.2	15.9
109.16	1841	109b	1.8	140.8	32.1	348.2	40.0	12.9
109.16	1841	109c	2.0	133.3	54.8	414.5	37.0	16.4
120.33	1816	120a	1.7	108.3	394.1	306.6	16.7	21.7
120.33	1816	120b	2.0	80.1	432.1	93.7	14.8	14.8
120.33	1816	120c	1.8	78.3	503.3	121.6	13.2	15.4
131.95	1788	131a	2.1	51.2	272.1	167.8	12.3	90.1
131.95	1788	131b	2.6	61.0	122.7	227.4	18.1	103.8
131.95	1788	131c	3.9	101.3	125.6	416.4	25.6	287.1
140.67	1765	140a	1.9	27.9	61.9	122.2	8.4	9.6
140.67	1765	140b	2.1	77.8	54.3	1905.3	19.1	21.5
140.67	1765	140c	2.3	105.9	59.9	2205.1	50.4	36.8
145.4	1753	145a	1.9	110.6	91.0	860.0	52.5	29.0
145.4	1753	145b	2.8	77.1	49.9	301.0	21.7	12.3
145.4	1753	145c	2.7	45.2	1245.7	358.9	102.7	66.7
158.74	1715	158a	1.9	16.2	57.9	7.5	20.8	23.8
158.74	1715	158b	2.1	32.0	171.6	10.4	40.0	55.7
158.74	1715	158c	1.9	20.7	40.2	8.6	28.1	17.1

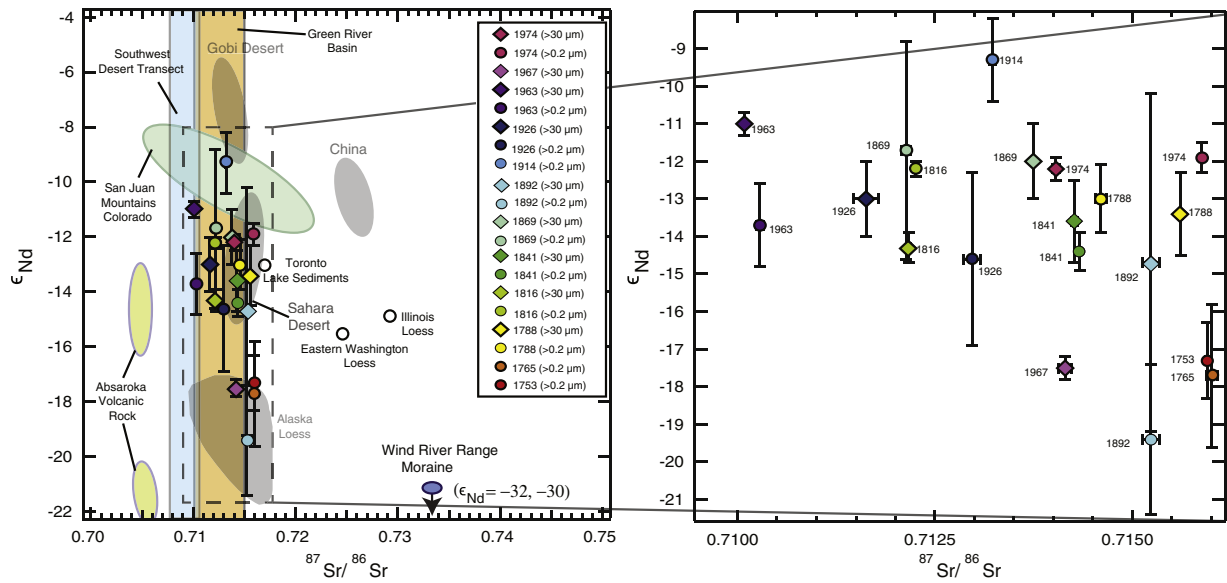


Fig. 11. ϵ_{Nd} and $^{87}\text{Sr}/^{86}\text{Sr}$ for dust within UFG ice (symbols) and for potential sources of dust to UFG (labeled symbols and coloured areas) (Ballantyne et al., 2011; Biscaye et al., 1997; Doebbert et al., 2014; Goldstein et al., 2008; Lawrence et al., 2011; Neff et al., 2008; Painter et al., 2007). For $^{87}\text{Sr}/^{86}\text{Sr}$ analytical errors are smaller than the graph symbols. The graph at the right is the zoomed in plot of ϵ_{Nd} and $^{87}\text{Sr}/^{86}\text{Sr}$ isotope compositions of dust. (For interpretation of the references to colour in this figure legend, the reader is referred to the web version of this article.)

less than $\text{PM}_{2.5}$ (in this case the rising abundance of small PM is $\sim 1.5 \mu\text{m}$) may be the result of an increase in anthropogenic pollutants (Rodriguez et al., 2011; Silva et al., 2013).

3.3. Trace element concentrations indicate anthropogenic influence

The crustal enrichment factor (EF) is defined here as the concentration ratio of a particular element relative to that of Al (which serves as

an indicator for rock and soil dust) in the ice, normalized to the same concentration ratio found in the upper continental crust (Wedepohl, 1995). For example, the EF for Pb is:

$$\text{EF}_c = \left(\frac{[\text{Pb}]_{\text{ice}}/[\text{Al}]_{\text{ice}}}{([\text{Pb}]_{\text{crust}}/[\text{Al}]_{\text{crust}})} \right)$$

The trace metal (Cr, As, Cd, Pb, Cu, and Zn) EF is represented in Fig. 10c, with a significant portion of the samples displaying EFs > 100

Table 2
Radiogenic isotopic compositions of UFG dust. ϵ_{Nd} and $^{87}\text{Sr}/^{86}\text{Sr}$ isotopic compositions of insoluble particle fraction extracted from UFG ice samples, reference materials and standards. F and C denote fine and coarse grained samples respectively. Numbers in parenthesis represent internal standard error.

Sample ID	Top depth (m)	Approximate age (yrs A.D.)	$^{87}\text{Sr}/^{86}\text{Sr} \pm 2\sigma 10^{-6}$	$^{143}\text{Nd}/^{144}\text{Nd} \pm 2\sigma 10^{-6}$	$\epsilon_{\text{Nd}} \pm 2\sigma$
21C	20.29	1974	0.714033 (40)	0.512015 (17)	-12.2 (0.3)
21F	20.29	1974	0.715880 (14)	0.512028 (21)	-11.9 (0.4)
30C	29.81	1967	0.714149 (79)	0.511742 (18)	-17.5 (0.3)
30F	29.81	1967	n.d.	n. d.	n.d.
33C	33.36	1963	0.710085 (24)	0.512076 (16)	-11.0 (0.3)
33F	33.36	1963	0.710283 (41)	0.511936 (58)	-13.7 (1.1)
62C	62.36	1926	0.711625 (164)	0.511974 (51)	-13.0 (1.0)
62F	62.36	1926	0.712970 (106)	0.511889 (115)	-14.6 (2.3)
70C	70.25	1914	0.713908 (38)	n. d.	n.d.
70F ^a	70.25	1914	0.713227 (42)	0.512164 (57)	-9.3 (1.1)
83C ^a	84.42	1892	0.716304 (168)	0.511883 (230)	-14.7 (4.5)
83F ^a	84.42	1892	0.715235 (108)	0.511646 (101)	-19.4 (2.0)
95C ^a	95.87	1869	0.713745 (21)	0.512025 (52)	-12.0 (1.0)
95F ^a	95.87	1869	0.712136 (58)	0.512040 (146)	-11.7 (2.9)
109C ^a	109.16	1841	0.714262 (38)	0.511938 (54)	-13.6 (1.1)
109F ^a	109.16	1841	0.714331 (17)	0.511902 (26)	-14.4 (0.5)
120C ^a	120.33	1816	0.712169 (16)	0.511906 (20)	-14.3 (0.4)
120F ^a	120.33	1816	0.712255 (19)	0.512014 (9)	-12.2 (0.2)
131C ^a	131.95	1788	0.715613 (23)	0.511951 (54)	-13.4 (1.1)
131F ^a	131.95	1788	0.714601 (67)	0.511970 (48)	-13.0 (0.9)
141C	140.67	1765	n. d.	n. d.	n.d.
141F ^a	140.67	1765	0.716006 (71)	0.511730 (98)	-17.7 (1.9)
145C	145.40	1753	0.715410 (191)	n. d.	n.d.
145F	145.40	1753	0.715946 (21)	0.511750 (50)	-17.3 (1.0)
158C	158.74	1715	0.710039 (481)	n. d.	n.d.
158F	158.74	1715	0.711767 (322)	n. d.	n.d.
BCR-2	-	-	0.705035 (7)	0.512642 (14)	0.1 (0.3)
BCR-2 ^a	-	-	0.705035 (7)	0.512634 (32)	-0.1 (0.6)
SRM987	-	-	0.710269(5)	-	-
JNdi-1	-	-	-	0.512102 (22)	-10.2 (0.4)

^a Denotes Nd measurements performed by TIMS equipped with 10^{13} Ohm resistors.

(Cr was the only trace metal with an EF measured at or below 9.3, see Table 1). EF greater than ten are possibly due to volcanic activity, forest fires, enrichment of certain metals in a source area, and long range transport of anthropogenic material (Gabrielli and Vallelonga, 2015). The very high crustal EFs in the samples may be attributed to interactions of insoluble dust with anthropogenic emissions as dust particles can scavenge pollutants during atmospheric transport and subsequently deposit them in terrestrial or aquatic ecosystems or upon ice sheets and glaciers (Erel et al., 2006; Reheis et al., 2009). We observe the highest crustal EFs (up to >100) for Pb and Cd most notably during 1753, 1765, and 1926 CE. The high crustal EFs in the older samples (1753 and 1765 CE) may be due to dust input from nearby sources enriched in these metals, as both samples have increasing input of particles >4 μm (Fig. 9). The sample from 1926 CE however, has increasing input of particles <2.5 μm (Fig. 9), and its high crustal EF could be a result of anthropogenic input (Table 1). Following the Clean Air Act of 1963, our observed crustal EFs are slightly lower, possibly a result of reduced air pollution emissions (Fig. 10c, see Table S1 for full TE concentrations).

3.4. Sr-Nd isotopic compositions as a tracer of variable dust provenance

Varying age and geologic history of continental crust results in unique Sr-Nd isotopic compositions for the source rock and resulting weathered material available for aeolian transport; these radiogenic isotopes are a powerful tool for determining dust provenance (Aarons et al., 2013; Abouchami et al., 2013; Biscaye et al., 1997; Bory et al., 2003, 2002; Gaiero, 2007; Grousset and Biscaye, 2005; Grousset et al., 1992, 1988, 1998; Kumar et al., 2014; Lupker et al., 2010). The Sr and Nd isotopic compositions of dust from the UFG ice, local potential dust material from the WRR, PSAs, and dust records from other American West regions are reported in Figs 10d,e and 11 (see Tables 2 and S2 for dust in ice and PSA isotope compositions respectively). Upper Fremont Glacier samples display a range of $^{87}\text{Sr}/^{86}\text{Sr}$ ratios: 0.71004 to 0.71630, and ϵ_{Nd} compositions: -9.3 to -19.4 . These radiogenic isotope data variations are large compared to ice core records from Greenland and Antarctica (variability of $^{87}\text{Sr}/^{86}\text{Sr} < 0.005$ and $\epsilon_{\text{Nd}} < 3$ in any single ice core record) (Delmonte et al., 2004a; Lupker et al., 2010). It is possible that each sample may represent ~ 1 year, and if this is indeed the case, the fluctuating radiogenic data indicates that dust provenance varied significantly over the last 300 years. It is also possible that the observed changes in isotopic composition are linked to changes in dust sources and pathways on seasonal timescales if individual samples span <1 year.

Samples with good agreement between the fine and coarse fraction in both Sr and Nd isotopic composition would suggest a local dust source. Based upon the PSA data available, this local dust source could be the Green River Basin, however sampling more PSAs from the surrounding areas would aid in the interpretation. Samples with the fine fraction displaying more radiogenic Sr isotopic compositions would imply input from a long range dust source (i.e. the Sahara); $^{87}\text{Sr}/^{86}\text{Sr}$ of dust particles is highly dependent upon the dust particle diameter and degree of weathering (Aarons et al., 2013; Biscaye, 1971). The $^{87}\text{Sr}/^{86}\text{Sr}$ and ϵ_{Nd} isotopic compositions of measured fine and coarse dust samples suggest potential mixing between dust originating primarily from the Colorado Plateau, American southwest deserts, the Green River Basin, and another dust source with similar Sr compositions and more radiogenic ϵ_{Nd} (Fig. 11). The combined Sr and Nd isotopic compositions of dust from the UFG are not in agreement with two separate WRR moraine samples, indicating that local input of dust from a recently exposed Little Ice Age moraine material is unlikely (Fig. 11).

The isotopic compositions suggest that the globally significant upwind northern hemisphere dust sources (e.g. deserts of Asia, Alaska loess) are not the dominant dust sources to this sector of the American West. Further, dust in these ice core samples have different isotopic compositions than dust deposited in the San Juan Mountains

sourced from the Colorado Plateau (Fig. 11) (Lawrence et al., 2011). The average $^{87}\text{Sr}/^{86}\text{Sr}$ and ϵ_{Nd} dust isotopic compositions from modern dust collectors in the WRR are 0.713 and -15 , respectively (Brahney et al., 2014), closely resembling the isotopic values of many younger UFG dust samples. We note that Sr isotope data for ancient Green River basin lake sediments have $^{87}\text{Sr}/^{86}\text{Sr}$ ratios ranging from 0.710 to 0.715, values that are well within the boundaries of the Sr isotopic composition measured here (Doebbert et al., 2014), although no published literature data is available for Nd compositions. Large increases in dust originating from the semi-arid portion of the Green River basin have occurred in the western US in the past few decades, including in the WRR, where dust deposition has doubled in the last decade (Brahney et al., 2013). Our most recent sample is from ~ 1974 CE, however it is possible that the increased dust input from the Green River basin extends to that time period. More recent samples from the UFG appear to be close in isotopic composition to one data point from the Green River basin, whereas the deeper, older samples originate from an uncharacterized source (Figs. 10d, 11). The oldest sample (158 m depth, ~ 1715 CE) has the lowest dust concentration and Sr isotopic composition, and one of the lowest crustal EF, which we would expect during a time period with low anthropogenic influence.

Combining radiogenic isotopic compositions with dust particle diameter is a complementary method of classifying variations in dust source and transport distance. Air masses may originate from Alaska, but it is unlikely that the coarse dust fraction is derived from such long-range sources. Depending on the wind speed (on average ranging from 3 to 12 m/s), gravitational settling should remove all of the 30 μm dust size fraction within 3000 km of the dust source (Aarons et al., 2013). Combined with observed isotopic similarities of the coarse and fine-fraction material, we conclude that the dust within the UFG ice is sourced primarily from the continental US. The exception may be several deeper/older samples (1753, 1765 and 1892 CE, fine fraction), displaying the most unradiogenic Nd compositions (Fig. 11). It is important to note that we do not have Nd isotope data of the coarse fractions of samples from 1753 and 1765 CE. The more contemporary and coarse fraction samples measure closer to the southwest desert and Colorado Plateau PSAs and modern dust measured in the WRR. Thus, our combined physical characterization-isotopic composition dataset may suggest a temporal shift in dust provenance to a more local source, although additional data is necessary to assess the statistical significance. This chemical proxy supports observational records indicating that over the last 100 years, changes in land use practices combined with cyclical droughts have resulted in dust transported thousands of kilometers across North America (Dean, 1997; Mahowald et al., 2005).

4. Conclusions

This work provides the first radiogenic isotope measurements of dust entrained in a midlatitude North American glacier. Our results serve as a preliminary survey of dust deposited on the UFG throughout the timescale in question, and provide evidence of a possible transition to relatively local dust input as the average dust particle diameter changes from ~ 2 to ~ 5 μm between 1815 and 1974 CE. More recent samples with increasing input of $\text{PM}_{2.5}$ may be an indication of particulate pollution from anthropogenic sources. The dust available for radiogenic isotope analysis in the UFG ice is two orders of magnitude less (e.g. <1 ng Nd) than dust measured in modern dust and lake sediment core studies, emphasizing the utility of applying new analytical techniques (10^{13} Ω resistors on TIMS) to small samples. The results presented here demonstrate the variable provenance of dust transported to this sector of the American West. This radiogenic isotopic composition dataset highlights the incomplete reference database of Sr-Nd isotopic measurements from PSAs in North America, which must be addressed before further source-to-sink analyses of aeolian dust.

Supplementary data to this article can be found online at <http://dx.doi.org/10.1016/j.chemgeo.2016.09.006>.

Acknowledgements

This research was funded by grants from the National Science Foundation EAR Division of Earth Sciences Award 1422473, the Geological Society of America Graduate Student Research Grant, the Rackham Graduate School at the University of Michigan and the Turner Award from the Department of Earth and Environmental Sciences at the University of Michigan. This is the Byrd Polar and Climate Research center contribution #1554. We would also like to thank the reviewers whose comments greatly improved this manuscript, and the drillers who retrieved and initially processed the ice core.

References

- Aarons, S.M., Aciego, S.M., Gleason, J.D., 2013. Variable Hf-Sr-Nd radiogenic isotopic compositions in a Saharan dust storm over the Atlantic: implications for dust flux to oceans, ice sheets and the terrestrial biosphere. *Chem. Geol.* 349–350, 18–26.
- Abouchami, W., et al., 2013. Geochemical and isotopic characterization of the Bodélé Depression dust source and implications for transatlantic dust transport to the Amazon Basin. *Earth Planet. Sci. Lett.* 380, 112–123.
- Ballantyne, A., et al., 2011. Biogeochemical response of alpine lakes to a recent increase in dust deposition in the Southwestern US. *Biogeosciences* 8, 2689–2706.
- Basile, I., et al., 1997. Patagonian origin of glacial dust deposited in East Antarctica (Vostok and Dome C) during glacial stages 2, 4 and 6. *Earth Planet. Sci. Lett.* 146 (3–4), 573–589.
- Belnap, J., Gillette, D.A., 1997. Disturbance of biological soil crusts: impacts on potential wind erodibility of sandy desert soils in southeastern Utah. *Land Degrad. Dev.* 8, 355–362.
- Betzler, P.R., et al., 1988. A pulse of Asian dust to the Central North Pacific: long range transport of giant mineral aerosol particles. *Nature* 314, 84–86.
- Biscaye, P.E., 1971. The rubidium, strontium, strontium-isotope system in deep-sea sediments: Argentine basin. *J. Geophys. Res.* 76, 5087–5095.
- Biscaye, P., et al., 1997. Asian provenance of glacial dust (stage 2) in the Greenland Ice Sheet project 2 ice core, Summit, Greenland. *J. Geophys. Res.* 102, 765–781.
- Bory, A.J.-M., Biscaye, P.E., Grousset, F.E., 2003. Two distinct seasonal Asian source regions for mineral dust deposited in Greenland (NorthGRIP). *Geophys. Res. Lett.* 30 (4).
- Bory, A.J.-M., Biscaye, P.E., Svensson, A., Grousset, F.E., 2002. Seasonal variability in the origin of recent atmospheric mineral dust at NorthGRIP, Greenland. *Earth Planet. Sci. Lett.* 196 (3–4), 123–134.
- Boutron, C.F., Patterson, C.C., Barkov, N.I., 1990. The occurrence of zinc in Antarctic ancient ice and recent snow. *Earth Planet. Sci. Lett.* 101 (2–4), 248–259.
- Brahney, J., Ballantyne, A.P., Sievers, C., Neff, J.C., 2013. Increasing Ca^{2+} deposition in the western US: the role of mineral aerosols. *Aeolian Res.* 10, 77–87.
- Brahney, J., et al., 2014. Dust mediated transfer of phosphorus to alpine lake ecosystems of the Wind River Range, Wyoming, USA. *Biogeochemistry* 120 (1–3), 259–278.
- Cecil, L.D., Vogt, S., 1997. Identification of bomb-produced chlorine-36 in mid-latitude glacial ice of North America. *Nucl. Inst. Methods Phys. Res. B* 123 (1–4), 287–289.
- Curtis, J., Grimes, K., 2004. Wyoming Climate Atlas.
- Dean, W.E., 1997. Rates, timing, and cyclicity of Holocene eolian activity in north-central United States: evidence from varved lake sediments. *Geology* 25 (4), 331–334.
- Delmonte, B., Petit, J.R., Maggi, V., 2002. Glacial to Holocene implications of the new 27000-year dust record from the EPICA Dome C (East Antarctica) ice core. *Clim. Dyn.* 18 (8), 647–660.
- Delmonte, B., et al., 2004a. Comparing the EPICA and Vostok dust records during the last 220,000 years: stratigraphical correlation and provenance in glacial periods. *Earth Sci. Res.* 66 (1–2), 63–87.
- Delmonte, B., et al., 2010. Aeolian dust in the Talos Dome ice core (East Antarctica, Pacific/Ross Sea sector): Victoria Land versus remote sources over the last two climate cycles. *J. Quat. Sci.* 25 (8), 1327–1337.
- Doebbert, A.C., et al., 2014. Controls on Sr isotopic evolution in lacustrine systems: Eocene green river formation, Wyoming. *Chem. Geol.* 380, 172–189.
- Donarummo Jr., J., Ram, M., Stoermer, E.F., 2003. Possible deposit of soil dust from the 1930's U.S. dust bowl identified in Greenland ice. *Geophys. Res. Lett.* 30 (6).
- Draxler, R.R., Hess, G.D., 1998. An overview of the HYSPLIT 4 modelling system for trajectories, dispersion, and deposition. *Aust. Meteorol. Mag.* 47, 295–308.
- Erel, Y., Dayan, U., Rabi, R., Rudich, Y., Stein, M., 2006. Trans boundary transport of pollutants by atmospheric mineral dust. *Environ. Sci. Technol.* 40 (9).
- Fischer, H., Siggaard-Andersen, M.-L., Ruth, U., Rothlisberger, R., Wolff, E., 2007. Glacial/interglacial changes in mineral dust and sea-salt records in polar ice cores: sources, transport and deposition. *Rev. Geophys.* 45.
- Fryxell, F., 1935. *Glaciers of the Grand Teton National Park of Wyoming*. J. Geol. 43 (4), 381–397.
- Gabrielli, P., Vallelonga, P., 2015. *Contaminant Records in Ice Cores, Environmental Contaminants: Using Natural Archives to Track Sources and Long-term Trends of Pollution*. Springer.
- Gaiero, D.M., 2007. Dust provenance in Antarctic ice during glacial periods: from where in southern South America? *Geophys. Res. Lett.* 34 (L17707).
- Ginoux, P., Prospero, J.M., Gill, T.E., Hsu, N.C., Zhao, M., 2012. Global-scale attribution of anthropogenic and natural dust sources and their emission rates based on MODIS Deep Blue aerosol products. *Rev. Geophys.* 50 (RG3005).
- Goldewijk, K., 2001. Estimating global land use change over the past 300 years: the HYDE database. *Glob. Biogeochem. Cycles* 15, 417–433.
- Goldstein, H., Reynolds, R., Reheis, M., Yount, J., Neff, J., 2008. Compositional trends in aeolian dust along a transect across the southwestern United States. *J. Geophys. Res.-Atmos.* 113.
- Grayson, D.K., 1993. *The Desert's Past: A Natural Prehistory of the Great Basin*. Smithsonian Institution Press, Washington, D.C.
- Grousset, F.E., Biscaye, P.E., 2005. Tracing dust sources and transport patterns using Sr, Nd and Pb isotopes. *Chem. Geol.* 222 (3–4), 149–167.
- Grousset, F.E., Biscaye, P.E., Zindler, A., Prospero, J., Chester, R., 1988. Neodymium isotopes as tracers in marine sediments and aerosols: North Atlantic. *Earth Planet. Sci. Lett.* 87, 367–378.
- Grousset, F.E., et al., 1992. Antarctic (Dome C) ice-core dust at 18 ky. B.P.: isotopic constraints on origins. *Earth Planet. Sci. Lett.* 111, 175–182.
- Grousset, F.E., et al., 1998. Saharan wind regimes traced by the Sr-Nd isotopic composition of the subtropical Atlantic sediments: last glacial maximum vs. today. *Quat. Sci. Rev.* 17, 395–409.
- Kampa, M., Castanas, E., 2008. Human health effects of air pollution. *Environ. Pollut.* 151, 362–367.
- Koornneef, J.M., Bouman, C., Schwieters, J.B., Davies, G.R., 2014. Measurement of small ion beams by thermal ionisation mass spectrometry using new 10^{13} Ohm resistors. *Anal. Chim. Acta* 819, 49–55.
- Kumar, A., et al., 2014. A radiogenic isotope tracer study of transatlantic dust transport from Africa to the Caribbean. *Atmos. Environ.* 82, 130–143.
- Lawrence, C., Neff, J., Farmer, G., 2011. The accretion of aeolian dust in soils of the San Juan Mountains, Colorado, USA. *J. Geophys. Res.-Atmos.* 116.
- Lupker, M., Aciego, S.M., Bourdon, B., Schwander, J., Stocker, T.F., 2010. Isotopic tracing (Sr, Nd, U and Hf) of continental and marine aerosols in an 18th century section of the Dye-3 ice core (Greenland). *Earth Planet. Sci. Lett.* 295, 277–286.
- Lyles, L., 1985. Predicting and controlling wind erosion. *Agric. Hist.* 59 (2), 205–214.
- Mahowald, N., et al., 1999. Dust sources and deposition during the last glacial maximum and current climate: a comparison of model results with paleodata from ice cores and marine sediments. *J. Geophys. Res.-Atmos.* 104 (D13), 15895–15916.
- Mahowald, N.M., et al., 2005. Atmospheric global dust cycle and iron inputs to the ocean. *Glob. Biogeochem. Cycles* 19.
- Middleton, N.D., Betzer, P.R., Bull, P.A., 2001. Long-range transport of 'giant' aeolian quartz grains: linkage with discrete sedimentary sources and implications for protective particle transfer. *Mar. Geol.* 177, 411–417.
- Naftz, D.L., 1993. *Ice-core Records of the Chemical Quality of Atmospheric Deposition and Climate from Mid-latitude Glaciers, Wind River Range, Wyoming*. Colorado School of Mines, Golden, CO 220 pp.
- Naftz, D., et al., 1996. Little Ice Age evidence from a south-central North American ice core. *U.S. Arct. Alp. Res.* 28, 35–41.
- Naftz, D.L., et al., 2002. Ice core evidence of rapid air temperature increases since 1960 in alpine areas of the Wind River Range, Wyoming, United States. *J. Geophys. Res.-Atmos.* 107 (D13).
- Neff, J.C., et al., 2008. Increasing eolian dust deposition in the western United States linked to human activity. *Nat. Geosci.* 1, 189–195.
- Painter, T., et al., 2007. Impact of disturbed desert soils on duration of mountain snow cover. *Geophys. Res. Lett.* 34.
- Patterson, E.M., Gillette, D.A., 1977. Commonalities in measured size distributions for aerosols having a soil-derived component. *J. Geophys. Res.* 82, 2074–2082.
- Prospero, J.M., Lamb, P.J., 2003. African droughts and dust transport to the Caribbean: climate change implications. *Science* 302, 1024–1027.
- Prospero, J.M., Ginoux, P., Torres, O., Nicholson, S.E., Gill, T.E., 2002. Environmental characterization of global sources of atmospheric soil dust identified with the Nimbus 7 Total Ozone Mapping Spectrometer (TOMS) absorbing aerosol product. *Rev. Geophys.* 40 (1).
- Reheis, M.C., 1997. Dust deposition downwind of Owens (dry) Lake, 1991–1994: preliminary findings. *J. Geophys. Res.-Atmos.* 102 (D22), 25999–26008.
- Reheis, M.C., Urban, F.E., 2011. Regional and climatic controls on seasonal dust deposition in the southwestern U.S. *Aeolian Res.* 3, 3–21.
- Reheis, M.C., Budahn, J.R., Lamothe, P.J., Reynolds, R.L., 2009. Compositions of modern dust and surface sediments in the Desert Southwest, United States. *J. Geophys. Res.* 114.
- Reynolds, R., Belnap, J., Reheis, M., Lamothe, P., Luiszer, F., 2001. Aeolian dust in Colorado Plateau soils: nutrient inputs and recent change in source. *Proc. Natl. Acad. Sci. U. S. A.* 98, 7123–7127.
- Rodriguez, S., et al., 2011. Transport of desert dust mixed with North African industrial pollutants in the subtropical Saharan Air Layer. *Atmos. Chem. Phys.* 11 (13), 6663–6685.
- Schepanski, K., Tegen, I., Laurent, B., Heinold, B., Macke, A., 2007. A new Saharan dust source activation frequency map derived from MSG-SEVIRI IR-channels. *Geophys. Res. Lett.* 34 (18).
- Schepanski, K., et al., 2009. Meteorological processes forcing Saharan dust emission inferred from MSG-SEVIRI observations of subdaily dust source activation and numerical models. *J. Geophys. Res.-Atmos.* 114.
- Schulz, M., Balkanski, Y., Guelle, W., Dulac, F., 1998. Role of aerosol size distribution and source location in a three-dimensional simulation of a Saharan dust episode tested against satellite derived optical thickness. *J. Geophys. Res.* 103 (D9), 10,579–10,592.
- Schuster, P., White, D., Naftz, D., Cecil, L., 2000. Chronological refinement of an ice core record at Upper Fremont Glacier in south central North America. *J. Geophys. Res.-Atmos.* 105, 4657–4666.
- Schuster, P., et al., 2002. Atmospheric mercury deposition during the last 270 years: a glacial ice core record of natural and anthropogenic sources. *Environ. Sci. Technol.* 36, 2303–2310.
- Schuster, P.F., et al., 2004. Fremont Glacier 1998 Core Tritium Data. IGBP PAGES/World Data Center for Paleoclimatology Data Contribution Series # 2004-079. NOAA/NGDC Paleoclimatology Program, Boulder CO, USA.

- Silva, R.A., et al., 2013. Global premature mortality due to anthropogenic outdoor air pollution and the contribution of past climate change. *Environ. Res. Lett.* 8 (3).
- Sugden, D.E., McCulloch, R.D., Bory, A.J.M., Hein, A.S., 2009. Influence of Patagonian glaciers on Antarctic dust deposition during the last glacial period. *Nat. Geosci.* 2 (4), 281–285.
- Tegen, I., Werner, M., Harrison, S.P., Kohfeld, K.E., 2004. Relative importance of climate and land use in determining present and future global soil dust emission. *Geophys. Res. Lett.* 31 (L05105).
- Thevenon, F., Anselmetti, F., Bernasconi, S., Schwikowski, M., 2009. Mineral dust and elemental black carbon records from an Alpine ice core (Colle Gnifetti glacier) over the last millennium. *J. Geophys. Res.-Atmos.* 114.
- Uglietti, C., Gabrielli, P., Cooke, C.A., Vallelonga, P., Thompson, L.G., 2015. Widespread pollution of the South American atmosphere predates the industrial revolution by 240 years. *Proc. Natl. Acad. Sci. U. S. A.* 112 (8).
- Uglietti, C., Gabrielli, P., Olesik, J.W., Lutton, A., Thompson, L.G., 2014. Large variability of trace element mass fractions determined by ICP-SFMS in ice core samples from worldwide high altitude glaciers. *Appl. Geochem.* 47, 109–121.
- Wedepohl, K.H., 1995. The composition of the continental crust. *Geochim. Cosmochim. Acta* 59, 1217–1232.
- Wolff, E.W., et al., 2006. Southern Ocean sea ice, DMS production and iron flux over the last eight glacial cycles. *Nature* 440 (7083), 491–496.
- Wong, G.J., Hawley, R.L., Lutz, E.R., Osterberg, E.C., 2013. Trace-element and physical response to melt percolation in Summit (Greenland) snow. *Ann. Glaciol.* 54 (63), 52–62.